

## Blue light activated photodegradation of biomacromolecules by N-doped titanium dioxide in a chitosan hydrogel matrix

Vittorio Ferrara<sup>a</sup>, Marco Marchetti<sup>b</sup>, Domenico Alfieri<sup>b</sup>, Lorenzo Targetti<sup>b</sup>, Michelangelo Scopelliti<sup>a</sup>, Bruno Pignataro<sup>a</sup>, Francesco Pavone<sup>c</sup>, Valeria Vetri<sup>a,\*</sup>, Giuseppe Sancataldo<sup>a</sup>

<sup>a</sup> Department of Physics and Chemistry - Emilio Segrè, University of Palermo, viale delle Scienze, Palermo 90128, Italy

<sup>b</sup> EmoLed S.r.l., Via di Rimaggio 141, Sesto Fiorentino, Florence 50019, Italy

<sup>c</sup> Department of Physics and Astronomy, University of Florence, via Giuseppe Sansone, Sesto Fiorentino, Florence 50019, Italy

### ARTICLE INFO

#### Keywords:

Photocatalysis  
Proteins  
Hydrogel  
Spectroscopy  
nitrogen-doped TiO<sub>2</sub>

### ABSTRACT

The use of photocatalysis activated by titanium dioxide nanostructured materials is a promising solution for many biomedical applications ranging from drug-free antibacterial to anticancer therapies, as well as for innovative hydrogel-supported phototherapies. This makes the effects of photocatalysis on the structure of biomolecules of a great relevance in order to define the applicability of photocatalytic materials in the biomedical fields. In this work, the effects of nitrogen-doped titanium dioxide (N-TiO<sub>2</sub>) dispersed in a biocompatible chitosan/PEG hydrogel on myoglobin and bovine serum albumin as target model proteins were investigated. The efficiency of this composite biocompatible material in inducing damages on biomolecules was assessed under blue light illumination by using spectroscopic techniques. N-TiO<sub>2</sub> nanoparticles were chosen as photocatalyst to trigger the photocatalytic process by irradiation with a blue light source, instead of higher energy sources, e.g. UV radiation, avoiding UV-related damages on biomolecules. In addition, the present work highlighted several advantages of using the hydrogel as medium for photocatalytic reactions. Firstly, N-TiO<sub>2</sub> nanoparticles were well dispersed and stabilized in the hydrogel respect to the correspondent aqueous suspension, and the photocatalytic reactions can occur in a biomimetic and biocompatible environment suitable for biomolecules, such as proteins. Importantly, the chitosan/PEG hydrogel enabled a direct investigation of the effects of photocatalysis on proteins by direct *in situ* spectroscopic measurements without any need of recovery of the target molecules, nor stirring during the photocatalysis, which could be detrimental for delicate biomolecules structures. Finally, the possibility to run *in situ* spectroscopic measurements directly in the N-TiO<sub>2</sub>-loaded hydrogel during the photocatalytic process allowed kinetic studies of photocatalytic process to obtain information of the chemical and structural modifications of proteins over time and not only at the end of the photocatalysis. Therefore, the reported results highlight the possibility of using this system as biomimetic environment to investigate the photocatalysis of proteins in detail overcoming relevant technical aspects that typically limit the study of photocatalysis of biomolecules, opening up the possibility to extend the approach to more complex biomolecular systems.

### 1. Introduction

Titanium dioxide (TiO<sub>2</sub>) and related materials are currently among the most effective photocatalysts, and they are widely exploited in several fields such as photovoltaics [1–3], cultural heritage [4–6], and environmental treatments [7–9]. Indeed, upon irradiation TiO<sub>2</sub>-based materials can induce photocatalysis, a light-triggered process consisting in the activation of a cascade of photochemical reactions mediated by

highly reactive radical species. Such radicals were produced in presence of a photocatalyst, whose electrons can be excited to the valence band by a radiation of proper wavelength. The resulting excitons determine an electrons transfer process to the surrounding chemical compounds at the catalyst interface yielding to radical species, as in an aqueous medium where most of the holes in the valence band can react with H<sub>2</sub>O or hydroxide ions (OH<sup>-</sup>) to produce hydroxyl radicals (OH·), and the electrons in the conduction band can reduce O<sub>2</sub> to produce superoxide ions

\* Corresponding author.

E-mail address: [valeria.vetri@unipa.it](mailto:valeria.vetri@unipa.it) (V. Vetri).

<https://doi.org/10.1016/j.jphotochem.2022.114451>

Received 25 July 2022; Received in revised form 10 November 2022; Accepted 22 November 2022

Available online 24 November 2022

1010-6030/© 2022 Elsevier B.V. All rights reserved.

(O<sub>2</sub>) [10]. Among the different materials, TiO<sub>2</sub> allotropes exhibit the simplest chemical composition, and they are generally applied in photocatalysis for their good properties in terms of photocatalytic efficiency, inexpensiveness, and nontoxicity.

These properties have stimulated a growing interest towards the use of TiO<sub>2</sub> in composites and colloids in Life Sciences [11]. In particular, several TiO<sub>2</sub>/polymer composites have been applied as coatings able to exploit the photochemical reactions induced by TiO<sub>2</sub> to damage biomolecules in viruses and bacteria, resulting in an effective antimicrobial activity [12–14].

The antimicrobial activity of TiO<sub>2</sub> has been widely demonstrated to induce death and reduce infection activity of both gram-positive and gram-negative bacteria, leading to the possibility to design effective sterilizing coatings against different human pathogen microorganisms [15–17]. Also, the possibility to inactivate phages by the use of TiO<sub>2</sub> films has been reported, and the capsid protein integrity has been indirectly shown to be affected by photocatalysis by using Bovine Serum Albumin (BSA) as radical scavenger [18].

As colloidal formulation, TiO<sub>2</sub> particles have shown the odds to use photocatalysis to design innovative antitumoral nanomaterials, as widely demonstrated against many types of cancer cells [19]. For this application, an interesting colloidal formulation consisting in antibody-bioconjugated TiO<sub>2</sub> nanoparticles specifically targeting brain cancer cells has been reported [20].

To properly design such bioactive platforms, elucidating the effects of photocatalysis on biological structures at the molecular level is of great relevance.

Several studies have made efforts in this direction, by evaluating the results by indirect tests, such as cell viability, proliferation assays, or formation of oxidation byproducts. For instance, studies on the effect of photocatalysis on the structure of bacteria membranes allowed to assess that the antimicrobial activity of photocatalysis is mainly due to peroxidation of membrane polyunsaturated phospholipids [21]. The phospholipids peroxidation, which induces structural changes and destabilization in the bacteria membrane, has been identified as the predominant mechanism in determining TiO<sub>2</sub> antibacterial effect [22–25].

Some efforts have been made towards a molecular insight on the effects of photocatalysis on proteins structure and function, as well. As an example, the structural changes on human serum albumin due to physisorption and photocatalysis at the surface of TiO<sub>2</sub> films were investigated by Raman spectroscopy, with interesting evidences of protein conformational changes [26]. The oxidative stress of proteins from fetal bovine serum has been evaluated upon treatment with TiO<sub>2</sub> by use of molecular biology techniques, in order to figure out the mechanism of protein corona formation on the particles surface in biological media [27,28]. Photocatalysis on free amino acids, as shown for cysteine [29], can also give additional information on the chemical pathways a more complex peptide or protein can undergo under irradiation.

Such molecular data result of high relevance to assess the safety of photoactive materials in a biological context [30], to enhance the effectiveness of TiO<sub>2</sub>-based materials in antitumoral and antimicrobial strategies [31], and to implement applications of photocatalysis even for environmental treatments and industry, for example, for protein degradation, as tested on model proteins such as lysozyme, BSA, and toxins [32,33], or to design advanced TiO<sub>2</sub>-loaded ultrafiltration membranes for removal of protein-based fouling from wastewater [34].

In this context, a simple and direct approach to directly monitor and investigate the chemical and conformational changes due to photocatalysis on biomolecules at molecular and supramolecular level is highly demanded. Especially for proteins, the study on the effects of photodegradation turns to be even more challenging whether information on the protein unfolding upon photocatalysis are required. Moreover, protein adsorption on the photocatalyst surface in a colloidal suspension further complicates the protein study after photocatalysis as leads to an impractical recover of the biomolecules from the system for

next analyses [35].

In the present study, the potentiality of nitrogen-doped titanium dioxide (N-TiO<sub>2</sub>) photocatalyst was exploited to set up a new system to investigate and directly monitor the chemical and conformational changes of proteins upon photocatalysis by a spectroscopic approach. The herein shown system was designed to overcome the typical issues of photocatalysis of biomolecules in order to obtain more detailed information on the effects of photocatalysis at molecular and structural level. To this aim, the N-TiO<sub>2</sub> powder and the target protein were dispersed in a biopolymeric hydrogel of chitosan (Ch) cross-linked with poly(ethylene glycol)diglycidyl ether (EPEG) [36]. Such composites of chitosan combined with TiO<sub>2</sub>-based structures characterized by photocatalytic activity constitute an interesting class of spreadable soft materials [37] for applications in the biological field, especially for antimicrobial treatments [38,39].

The entrapment of both N-TiO<sub>2</sub> and protein molecules in a hydrogel network is an ease and biocompatible way to solve different technical issues encountered in studying protein photocatalysis. Firstly, the hydrogel environment is highly hydrated, this being fundamental to maintain native-like conformation in proteins. Several hydrogels have been successfully applied as media for proteins loading, especially for protein conformational studies [40,41], as well as in controlled release experiments [42–44]. These systems have shown the feasibility of protein loading in hydrogel with protein activity retention, and the possibility to investigate structural changes, aggregation and fibrillation processes induced in an intracellular-mimicking hydrated environment. In particular, chitosan hydrogels attracted a remarkable interest as they represent an interesting biocompatible and highly hydrated three-dimensional network [45]. They contain large amounts of water, thus resembling biological tissues, and have demonstrated to be particularly suitable for proteins entrapment [46,47]. In addition to the above mentioned chitosan hydrogels properties, the Ch/PEG hydrogel shows the advantage to be a light-transparent network not interfering with N-TiO<sub>2</sub> activation by blue light, and it is suitable for study protein states by means of UV-visible absorption and fluorescence spectroscopies, with no need of protein recovery procedures.

Also, the encapsulation of the photocatalyst in a hydrogel represents a strategy to overtake limitations typical of colloidal suspensions, which in this specific case is represented by the tendency of N-TiO<sub>2</sub> to precipitate in aqueous media. As an alternative, stirring can limit the photocatalyst sedimentation, but can at the same time induce undesired structural changes in proteins, as unfolding or aggregation due to shear forces [48,49]. The possibility to use a stable dispersion of N-TiO<sub>2</sub> instead of TiO<sub>2</sub> represents a further advantage, since the former photocatalyst is well-known to be triggered under visible light irradiation [31,50]. In fact, the use of a UV source to activate TiO<sub>2</sub>, whose band gap is in the range 3.4–3.1 eV, corresponding to wavelength of 365–400 nm [51], represents a major limit for TiO<sub>2</sub> practical application in biological systems [52,53]. Doping the TiO<sub>2</sub> structure with nonmetal elements such as carbon, nitrogen, sulfur and phosphorus is the most exploited strategy to synthesize visible-light sensitive materials [54–58]. In particular, using nitrogen as doping agent is among the most pursued choice, because of its promising characteristics, such as easy introduction of nitrogen atoms through a simple aqueous sol-gel synthesis in presence of inexpensive chemicals as nitrogen source, e.g. urea, ammonia, ammonium salts [59].

Upon the N-TiO<sub>2</sub> and protein loading in the Ch/PEG hydrogel, the photocatalytic process was activated by irradiation with a blue light LED centered at 420 nm. Here, globular proteins, such as Myoglobin and BSA were chosen as model proteins for their structural and chemical stability, as well as for their well characterized oxidation and conformational states in aqueous solutions and hydrogels [41,60]. The photocatalysis effects on protein structure were investigated by means of UV-visible absorption and fluorescence *in situ* measurements in the N-TiO<sub>2</sub>-loaded hydrogel. This strategy successfully allows for an in-depth investigation of the effects of photocatalysis on model proteins, with the possibility to

extend the approach to study photocatalysis effects on more complex biomolecular systems. Also, reported N-TiO<sub>2</sub>-loaded Ch/PEG hydrogel can represent a relevant biocompatible system to be applied as new photoactive gel for antimicrobial applications in skin infections treatment and biofilm degradation.

## 2. Materials and methods

### 2.1. Materials

Titanium (IV) isopropoxide (TIPP, 97 %), isopropyl alcohol ( $\geq 99.8$  %), urea (suitable for cell culture), chitosan (Ch, medium molecular weight, 75–85 % *N*-deacetylated), poly(ethylene glycol)diglycidyl ether (EPEG, average  $M_n$  500), glacial acetic acid (AcOH,  $\geq 99$  %), methyl orange (for microscopy), Myoglobin (from equine skeletal muscle, 95–100 %), albumin (BSA, from bovine serum, > 96 %) were all purchased by Sigma Aldrich. Ultrapure water (Smart2Pure filtration system, Thermo Fischer Scientific Inc., 18.2 M $\Omega$ ) was utilized for all the solutions preparation.

### 2.2. N-TiO<sub>2</sub> synthesis and Characterization.

N-TiO<sub>2</sub> was prepared by a sol-gel synthesis with urea as nitrogen source. The Ti/N molar ratio was set at 1:6, to maximize the catalytic efficiency [56]. In a typical experiment, 4 mL of titanium (IV) isopropoxide were added dropwise to a mixture of isopropyl alcohol/water 1:10 v/v. Then, 3.75 mL of 10 M aqueous urea was added drop by drop, and the suspension kept under vigorous stirring for 4 h. The mixture was dried at 100 °C overnight, and calcined at 400 °C for 3 h. The yellow powder was crushed and washed by sonication in acetone, ethanol, and water for 1 h each. The undoped TiO<sub>2</sub> was synthesized through the same protocol, with no addition of urea, and used as reference.

The N-TiO<sub>2</sub> powder was characterized by FTIR by using a Bruker ATR FTIR spectrometer, model Alpha in attenuated total reflection (ATR) mode, equipped with a diamond interface. Spectra were acquired in the range 4000–400 cm<sup>-1</sup> with a resolution of 2 cm<sup>-1</sup> and an average of 64 scans each.

X-ray Photoelectron Spectroscopy (XPS) spectra were recorded with a PHI 5000 VersaProbe II scanning XPS microprobe (ULVAC-PHI, Chigasaki, Japan) using a monochromatic X-ray source (Al K $\alpha$ ,  $h\nu = 1486.6$  eV). Electrons were collected using a 100  $\mu$ m diameter beam (25 W, 15 kV) and a hemispherical analyzer operating in FAT mode, angled at 45° with respect to the analyzed surface. During all collections, both electrons and Ar<sup>+</sup> ions were used to compensate superficial charging. Survey spectra were collected with a pass energy (PE) of 117.500 eV and an energy resolution of 1.000 eV; high resolution spectra were collected with a PE of 23.5 and an energy resolution of 0.500 eV. Obtained binding energy values are referred to adventitious carbon (284.80 eV) used as internal reference.

The particles size was obtained in acidic suspension of HCl (pH 2) by a Zetasizer Nano ZS Malvern instrument at 25 °C with an equilibration time of 180 s. Each size measurement was obtained as the mean of 10 runs with duration time of 10 s. The sample was also imaged by Scanning Electron Microscopy (SEM) by drop casting the acidic particles suspension on a metallic stub to dry the sample overnight at room temperature. The sample surface was sputter-coated with gold before SEM imaging. The SEM images were acquired by a FEI Versa 3D microscope at an accelerated voltage of 20 kV, current of 27 pA, and magnification of 20 000 $\times$  and 40 000 $\times$ .

The nanostructure of the nanoparticles was also investigated by Atomic Force Microscopy (AFM). Sample solution used for DLS was diluted 1:10 000 and 20  $\mu$ l aliquots were drop casted on freshly cleaved mica and dried on air at room temperature. The AFM images were acquired in air by means of a Bruker FAST-SCAN microscope equipped with a closed-loop scanner. The scans were obtained in tapping mode by using FAST-SCAN-A probes with apical radius of about 5 nm. Each AFM

image was obtained with a pixel resolution comparable to the tip size. The diameter of the nanoparticles was estimated by evaluating their height from the AFM scans.

UV-vis diffuse reflectance spectra were recorded by using a UV-vis-NIR V-770 Jasco spectrophotometer equipped with a 60 mm integrating sphere (ISN-923). Photocatalyst powder was placed in the solid sample holder and measurements were performed in the range 200–800 nm by setting a scan speed of 100 nm/min and a bandwidth of 2 nm. The Kubelka-Munk transformation was applied to the retrieved data to calculate the photocatalyst band gap energy. [51].

### 2.3. Hydrogel preparation and Loading.

N-TiO<sub>2</sub> powder was dispersed in a chitosan solution (3 % w/v in AcOH 1 % v/v), and an equal volume of pure EPEG was added to induce the gelification process at 65 °C for 1 h. The amount of N-TiO<sub>2</sub> loaded in the gel is 20 mg/mL respect to the final hydrogel volume. The resulting hydrogel was soaked overnight in an aqueous solution of the target molecule, such as methyl orange (50 mg/L), Myoglobin (2 mg/mL), or of BSA (1 mg/mL). The volume of solution is 5 times the volume of the hydrogel to induce both hydrogel swelling and target molecules loading. Reference hydrogel with no addition of N-TiO<sub>2</sub> was prepared and loaded with target molecules by the same protocol.

### 2.4. Photocatalysis

The photocatalytic process was activated by exposing the N-TiO<sub>2</sub>/hydrogel loaded with the target molecule to a LED emitting in the blue spectral region (Lumileds, L1CU-VLT1000000000). The LED spectrum was recorded by an Avantes multichannel spectrometer AvaSpec-3648 (Figure S1A).

All the photocatalysis experiments were carried out by exposing samples to the LED light at 2 cm distance (scheme of the experimental setup in Figure S1B). The power of the blue LED was measured at 2 cm distance by using a standard silicon calibration cell through a tester and a value of 8 mW/cm<sup>2</sup> was recorded.

At first, methyl orange photostability under blue light exposition was tested by measuring absorption spectra of a 3 mL solution in a quartz cuvette (optical path 1.00 cm) at different time of irradiation (Figure S2). Then, methyl orange dye (50 mg/L) was used for reference photocatalysis experiments performed in aqueous suspension of N-TiO<sub>2</sub> (10 mg/mL) by keeping the system under continuous stirring. A centrifugation step at 6000 rpm for 10 min was needed to remove out the photocatalyst particles before recording absorption spectra of 3 mL of the supernatant solution in a quartz cuvette (optical path 1.00 cm).

The stability of the Ch/PEG hydrogel after 10 days of storage in the dark at room temperature without irradiation was firstly evaluated by UV-vis spectroscopy (Figure S3). Thus, experiments in hydrogel were carried out by filling a quartz cuvette (optical path 0.50 mm) with the N-TiO<sub>2</sub>-loaded hydrogel loaded containing the target molecule, then exposing the sample to the LED light. The same protocol was applied to assess the hydrogel (Figure S4) and aqueous Myoglobin (1 mg/mL) (Figure S5) photostability under blue light irradiation in the herein tested experimental conditions. Absorption and fluorescence spectra were carried out directly on the cuvette containing the hydrogels at different irradiation times.

### 2.5. Absorption measurements

Photocatalysis effects were evaluated by UV-vis absorption spectroscopy using a UV-vis-NIR V-770 Jasco spectrophotometer. Spectra of the solutions and hydrogels were recorded in 1.00 cm and 0.50 mm optical path quartz cuvettes, respectively. Spectra were acquired in the range 200–800 nm, with a bandwidth of 2.0 nm, and a scan speed of 200 nm/min.

## 2.6. Fluorescence spectra

The steady-state fluorescence measurements were carried out in the range of 300–550 nm using a Jasco-FP-8500 spectrofluorometer by setting the excitation wavelength ( $\lambda_{ex}$ ) at 280 nm, the excitation and emission bandwidth at 2.5 nm, and a scan speed of 200 nm/min. Spectra of the hydrogels were recorded in 0.50 mm optical path quartz cuvettes. The cuvette was placed in a sample holder and positioned at 90° respect to the detector for fluorescence measurements.

## 3. Results and discussion

In the present work a Ch/PEG hydrogel loaded with the blue light sensitive N-TiO<sub>2</sub> photocatalyst was applied as biocompatible medium for studying the photocatalysis of model globular proteins, such as equine skeletal muscle Myoglobin and BSA. In Fig. 1, a scheme of the main steps of the sol-gel synthesis optimized to obtain the N-TiO<sub>2</sub> nanoparticles, as well as the Ch/PEG formation step and protein loading were drawn.

The N-TiO<sub>2</sub> photocatalyst was synthesized by a sol-gel method by using urea as a nitrogen source (Fig. 1A). The method offers the possibility to obtain a blue light sensitive photocatalyst by a simple approach, with no use of hazardous chemicals. Urea decomposition can be used as a convenient strategy for the *in situ* production of ammonia [61] during the calcination process, leading to nitrogen incorporation in the TiO<sub>2</sub> lattice.[56] Then, the obtained N-TiO<sub>2</sub> particles were dispersed in the chitosan/EPEG solution and the gelation process was thermally induced (Fig. 1B). The N-TiO<sub>2</sub>-loaded Ch/PEG was soaked in the target molecule solution overnight to induce the hydrogel swelling and the molecules loading.

### 3.1. Characterization of N-TiO<sub>2</sub>

The obtained N-TiO<sub>2</sub> powder was characterized in terms of chemical composition, particles size and interaction with UV-visible light.

Firstly, the chemical composition of the N-TiO<sub>2</sub> powder was

investigated by means of ATR FTIR and XPS spectroscopies. These measures are aimed at investigating the N-TiO<sub>2</sub> chemical properties by comparison with the reference pristine TiO<sub>2</sub>.

In Fig. 2A, FTIR measurements in ATR mode are reported. According to the literature, the ATR FTIR spectrum of the undoped TiO<sub>2</sub> is characterized by typical broad absorption band at around 3400 cm<sup>-1</sup> and by a sharper band at 1630 cm<sup>-1</sup> attributed to symmetric and asymmetric stretching vibrations, and bending of O–H bonds, respectively. The former signal is related to O–H vibrations in titanol groups and surface adsorbed water molecules, the latter signal is due to moisture [62]. A strong absorption band is also observed from 1100 cm<sup>-1</sup> ascribed to stretching modes characteristic of the Ti–O bonds [63]. In the observed spectral region TiO<sub>2</sub> and N-TiO<sub>2</sub> are almost superimposable. An additional narrow absorption peak at 2050 cm<sup>-1</sup>, related to -N=N- bond stretching and reported for some N-TiO<sub>2</sub> samples [64,65], is observed confirming the efficiency of the doping process.

The chemical composition of the TiO<sub>2</sub> and N-TiO<sub>2</sub> powders was analyzed by means of XPS. The comparison of the two XPS surveys spectra of TiO<sub>2</sub> and N-TiO<sub>2</sub> in Fig. 2B, besides the expected Ti, O and C peaks, showed as a main difference a peak in the N 1s region (around 400 eV). Such a region was further analyzed at higher resolution (Fig. 2C), showing the presence of two main components: a typical “organic nitrogen” at 400 eV, attributable to aminic/amidic nitrogen, and a second peak (397.5 eV) characteristic of a metal bound N atom [56,66,67]. The second component demonstrates the successful synthesis of the N-TiO<sub>2</sub>, as clearly shows the presence of nitrogen doping agent atoms directly bound to the metal titanium atoms.

In addition, characterization of the N-TiO<sub>2</sub> particles size was carried out by dynamic light scattering (DLS) measurements upon suspension in an acidic medium, SEM and AFM.

The low pH allows DLS measurements by slowing the sedimentation process through the electrostatic stabilization of the particles [68,69]. In Fig. 3A the size of the N-TiO<sub>2</sub> and TiO<sub>2</sub> particles suspended in HCl (pH 2) is shown. The size distribution of the particles reveals a hydrodynamic diameter centered at 250 nm for the undoped material with a polydispersity index of 0.185. For the N-TiO<sub>2</sub> particles the hydrodynamic

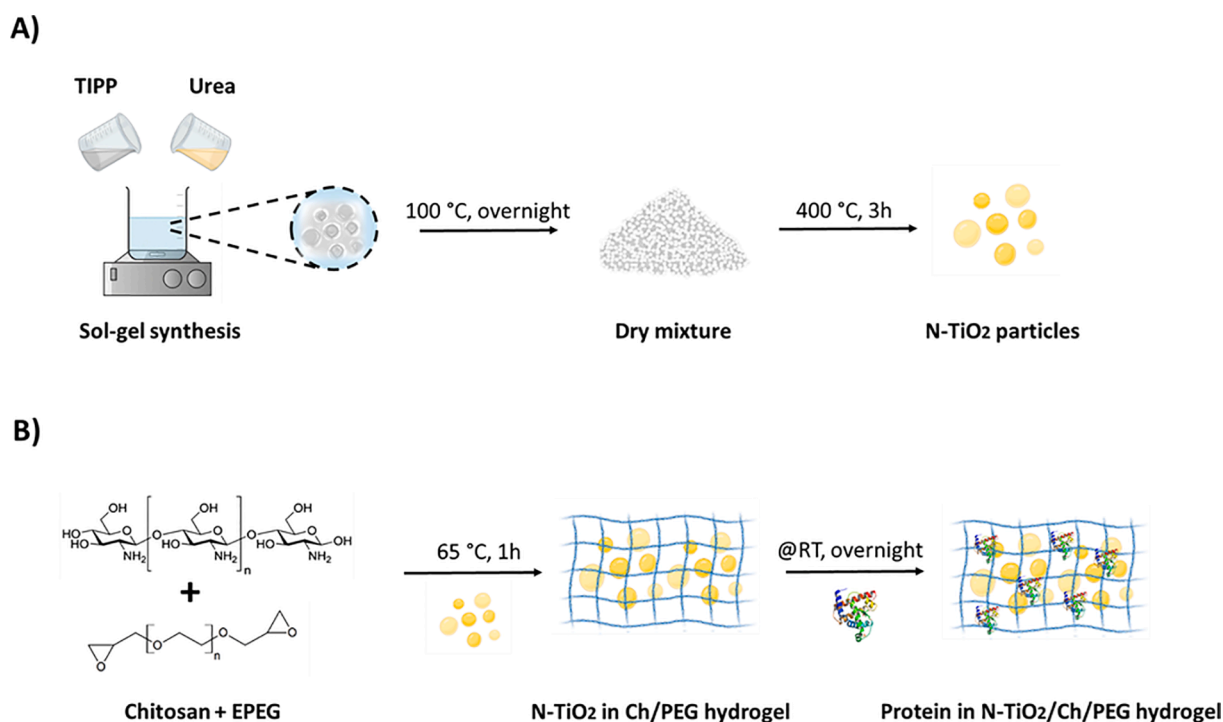


**Fig. 1.** Schematic representation of A) synthesis of the N-TiO<sub>2</sub> photocatalyst through the sol-gel approach, and B) scheme of the Ch/PEG hydrogel preparation and trapping of N-TiO<sub>2</sub> nanoparticles (yellow spheres) and of the target protein.

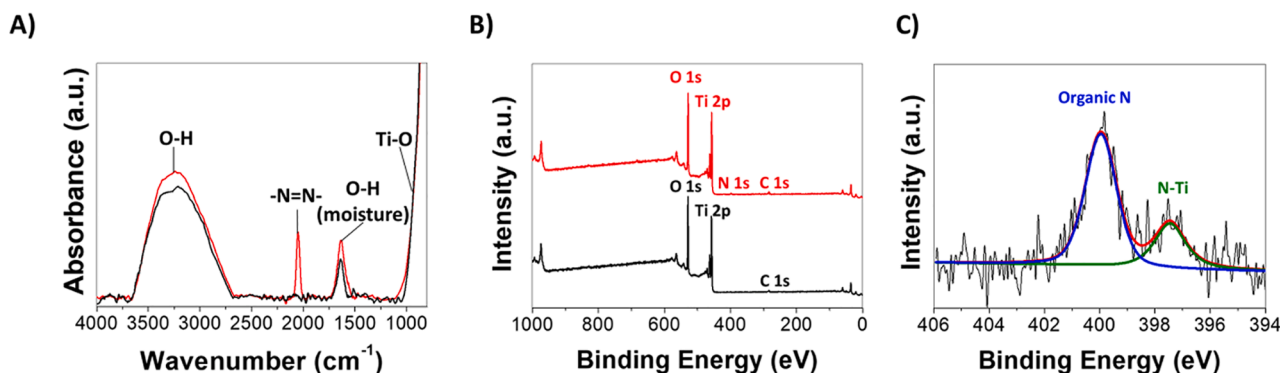


**Fig. 2.** Chemical characterizations of N-TiO<sub>2</sub> particles (red) by using the undoped TiO<sub>2</sub> (black) as reference: A) ATR FTIR spectra in the range 4000–800 cm<sup>-1</sup>, and B) XPS survey spectra in the range 1000–0 eV. In panel C) the high-resolution N 1s peak of N-TiO<sub>2</sub> analyzed as a sum of two components at 400.0 eV (blue line) and 397.5 eV (green line), corresponding to organic N and N-Ti components, respectively.

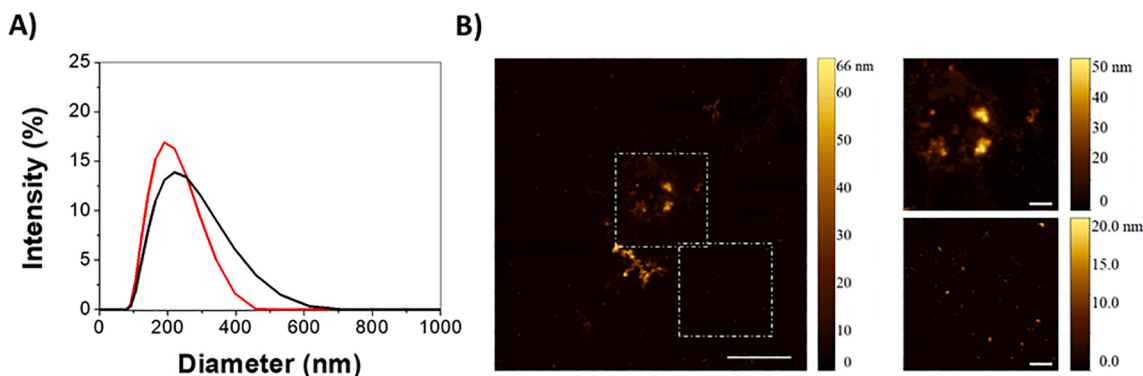


**Fig. 3.** Size characterization of N-TiO<sub>2</sub> particles (red) by using the undoped TiO<sub>2</sub> (black) as reference: A) size of purified particles (0.01 mg/mL) dispersed in aqueous HCl at pH 2 determined by DLS measurements, and B) representative AFM image of N-TiO<sub>2</sub> particles (scale bar 1 μm) with dashed squares select regions corresponding to the zoom of areas showing larger clusters and free nanoparticles (scale bars 200 nm).

diameter is smaller, with a maximum in the size distribution at 200 nm and a polydispersity index 0.093.

The particles size of the N-TiO<sub>2</sub> photocatalyst was also investigated by SEM, as shown in Figure S6. In accordance with DLS, the N-TiO<sub>2</sub> particles deposited on a metallic support in the dry state exhibit an irregular shape, in some cases characterized by sharp edges, with a diameter in the range of 100–350 nm.

To further characterize the structure of the N-TiO<sub>2</sub> particles at the nanoscale, AFM measurements were performed. In Fig. 3B a representative AFM measurement of the N-TiO<sub>2</sub> is reported, along with zoom of selected areas to evidence the presence of two different particles populations. In particular, the AFM analysis of the sample evidenced the presence of both large clusters with characteristic size in the scale of ~200 nm, and smaller isolated nanoparticles. To further investigate the particles size, the height profiles of the sample in different regions were measured, as reported in Figure S7. These measurements highlighted that the smaller particles are characterized by a height in the range of 10–20 nm (blue lines), and that the larger structures obtained by smaller particles clustering, are characterized by a height in the range of 30–50 nm (green lines).

Taken together these measurements support the evidence that multiple nanoscale species are present in the photocatalyst sample. Both large aggregates and small isolated nanoparticles are found. Likely, the large aggregates consist in clusters of smaller nanoparticles, obtained during the calcination step at 400 °C at the end of the sol-gel synthesis. Indeed, the clustering of nanoparticles through sintering during thermal treatments is a common phenomenon for TiO<sub>2</sub>-based nanomaterials [70–73]. Therefore, we can conclude that the N-TiO<sub>2</sub> powder here reported shows a structure at the nanoscale that is typically observed for

TiO<sub>2</sub>-based materials.

Finally, a fundamental characterization of the N-TiO<sub>2</sub> is the evaluation of its interaction with light. The energy necessary for the photocatalyst to be activated depends on the band gap value, which in turns determines the wavelength of the irradiation light. Compared to the undoped material, which is typically white, the nitrogen doping of TiO<sub>2</sub> structure led to a yellow powder (Chromaticity diagram CIE 1930 in Figure S8), suggesting a band gap narrowing. The optical properties of both N-doped and undoped materials were determined by UV-vis diffuse reflectance spectroscopy. In Fig. 4A, the reflectance spectra confirm that N-TiO<sub>2</sub> sample has modified optical properties with respect to the pristine TiO<sub>2</sub>.

As expected, the undoped TiO<sub>2</sub> is characterized by a high reflectance in the whole visible range (400–800 nm). A critical decay of the signal is observed for wavelengths above 350 nm, whilst, as expected, the decay of diffuse reflectance intensity is red shifted for N-TiO<sub>2</sub> [56,65]. These data are in line with previously reported measurements, and clearly indicate that the new material absorbs in the visible blue light spectral range. By the reflectance spectra it is possible to calculate the band gap energy of the photocatalysts by using the Kubelka–Munk method [51]. The band gap energy calculated is 3.1 eV for the undoped TiO<sub>2</sub>, in accordance with reported values [51], and 2.8 eV for N-TiO<sub>2</sub>. A scheme of the effect of the nitrogen atoms in the TiO<sub>2</sub> structure on the band gap values is drawn in Fig. 4B. In terms of wavelength, the band gap energies correspond to 400 nm and 442 nm, respectively. Therefore, the N-TiO<sub>2</sub> offers the possibility to use a blue light instead of a radiation in the UV range for the material activation.

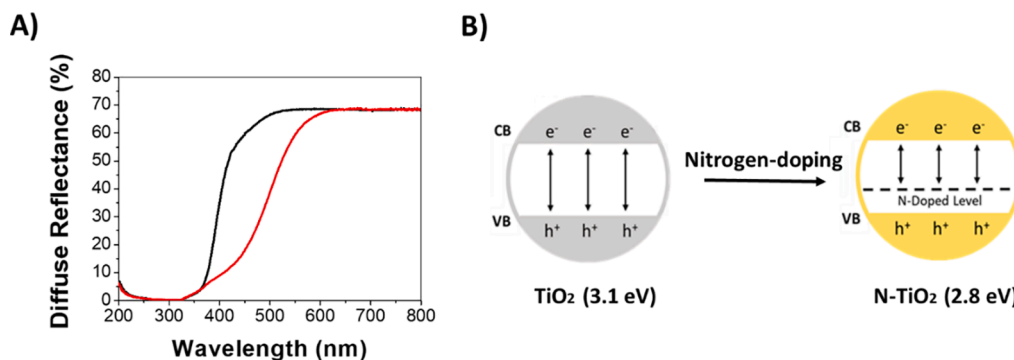


Fig. 4. N-TiO<sub>2</sub> (red) and undoped TiO<sub>2</sub> (black) A) UV-vis diffuse reflectance spectra in the range 200–800 nm, and B) relative scheme of the effect of the nitrogen-doping process on the TiO<sub>2</sub> band gap value. VB and CB labels indicates the valence and conduction bands.

### 3.2. N-TiO<sub>2</sub> photocatalytic properties

The first step in the present study consisted in the evaluation of the photocatalytic properties of the N-TiO<sub>2</sub> powder activated by irradiation. The photocatalytic efficiency of N-TiO<sub>2</sub> was firstly evaluated in an aqueous suspension of methyl orange dye, a small organic molecule. Assessing the photocatalytic properties of materials by means of the use of this dye is a widely used method in this field both for life and material science applications [74–76]. In the selected experimental conditions this dye is highly stable under illumination at 420 nm. Changes in methyl orange spectrum, both in terms of shape and intensity, are related to the degradation of the dye, due to radical photocatalytic reactions [77].

Methyl orange (50 mg/mL) in aqueous suspension containing 10 mg/mL N-TiO<sub>2</sub> was uniformly illuminated for 18 h under stirring. At selected time points, the irradiated sample was spun down and the supernatant was recovered. In Fig. 5A, UV-vis absorption spectra of the isolated methyl orange solution at defined time points are reported.

As it is evident, the initial spectrum of methyl orange dye (black line) shows the characteristic absorption band of the dye [78,79]. As can be seen, this band undergoes critical modifications: the peak decreases in intensity and undergoes a blue shift along with relevant bands shape modification. The observed modifications are in line with the ones reported in the literature as a consequence of molecular degradation due to the photocatalytic reactions [80–82]. The change in the band shape can be attributed to the several methyl orange byproducts obtained during the photocatalytic process, which activates a cascade of chemical degradation pathways [74]. A qualitative estimation of the velocity of the photodegradation induced by N-TiO<sub>2</sub> is reported in Fig. 5B, where the decay of the absorbance value measured at 464 nm is shown. These results confirm photocatalytic effectiveness of the N-TiO<sub>2</sub> as illuminated

with blue light.

As performing the analysis in aqueous suspension, sedimentation of the N-TiO<sub>2</sub> readily occurs. This does not constitute a technical problem when analyzing small soluble molecules, as the solution can be easily stirred without inducing damages to the sample. However, to analyze molecules characterized by higher complexity, like proteins, stirring procedure may be not desirable as it can induce protein unfolding or aggregation due to shear forces [48,49].

Then, the possibility to investigate photocatalysis processes on bio-molecules encapsulated in the Ch/PEG hydrogel was explored. This chemical hydrogel was obtained by chitosan crosslinking with EPEG, an epoxy-terminated PEG derivative, and the success of the crosslinking reaction was assessed by UV-vis absorption spectroscopy. For the Ch/PEG hydrogel a characteristic absorption band at 305 nm was observed, which can be related to the crosslinking bonds formed through the reaction of the chitosan primary amino groups and the reactive epoxide rings at the EPEG termini [83]. The chemicals involved in the hydrogel synthesis do not present absorption in this spectral region (Figure S9).

Also, the Ch/PEG hydrogel was chosen as it presents suitable properties as dispersing medium for N-TiO<sub>2</sub> powder and as protein encapsulating network, as well as for its good photostability, and reduced degradability during photocatalysis induced by N-TiO<sub>2</sub> in the present experimental conditions.

To test the effects of photocatalysis on the matrix, the hydrogel was loaded with N-TiO<sub>2</sub> (20 mg/mL), then exposed to blue light LED over time (Figure S10). In the observed experimental conditions, the larger observed change consists in an initial decrease after 1 h of irradiation of the main peak centered at about 305 nm. For longer irradiation time this absorption peak did not show any further modifications. This effect was ascribed to a hydrogel structural rearrangement, e.g. swelling/equilibrium to the experimental conditions. The Ch/PEG hydrogel in these

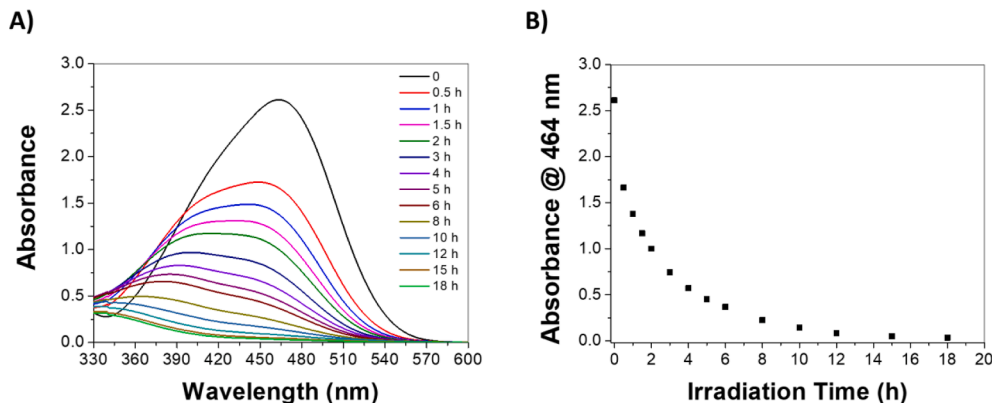


Fig. 5. A) UV-vis absorption spectra in the range 330–600 nm of methyl orange (50 mg/L) supernatant recovered from aqueous suspension containing 10 mg/mL N-TiO<sub>2</sub> at different irradiation time points, and B) time evolution of absorbance measured at  $\lambda = 464$  nm.

conditions presents a suitable stability to further modifications due to photocatalytic reactions.

Remarkably, the N-TiO<sub>2</sub>-loaded hydrogel does not present absorption in the visible spectral region. In addition, no significant fluorescence emission signal was detected from the hydrogel under excitation at  $\lambda_{\text{ex}}$  of 280 nm (Figure S11).

These features highlighted that the N-TiO<sub>2</sub>-loaded Ch/PEG hydrogel is a potential photocatalytic material, in terms of both stability to photocatalysis and transparency to visible light, confirming its suitability for further absorption and fluorescence experiments in the visible range by a simple spectroscopic approach.

The photocatalytic activity of N-TiO<sub>2</sub> was at first tested on the model dye methyl orange loaded in the hydrogel matrix. In Fig. 6A, the absorption spectra of methyl orange trapped in the N-TiO<sub>2</sub>-loaded hydrogel is shown at different time points during the exposure to blue LED light.

Before the photocatalysis process was activated, the spectrum of methyl orange (Fig. 6A, black line) showed analogous spectral features of the correspondent spectrum in suspension (Fig. 5A, black line). The absorbance value measured at  $\lambda = 464$  nm for the methyl orange in the N-TiO<sub>2</sub>-loaded hydrogel was 0.18, which corresponds to the expected value calculated with an optical path of 0.50 mm and a molar extinction coefficient  $\epsilon_{\text{MO}} = 25\,100\text{ M}^{-1}\text{cm}^{-1}$  [84].

Upon irradiation, it is evident that the absorption spectrum of the dye undergoes critical modifications as a function of time. In particular, a decrease in intensity and a blue-shift with relevant shape modification for the band at  $\lambda = 464$  nm is observed. The same is also observed for the component at  $\lambda = 424$  nm which flattens and blue-shifts during photocatalysis. These data clearly evidence the photocatalytic activity of N-TiO<sub>2</sub> in the Ch/PEG hydrogel matrix, and the suitability of the system to catalyze photodegradation of organic compounds.

In addition, comparing the photocatalysis of methyl orange in aqueous suspension in Fig. 5A and the corresponding process in the Ch/PEG hydrogel in Fig. 6A, it is possible to observe that similar modifications of the UV-vis absorption spectra of methyl orange occur over time both in aqueous suspension and in the hydrogel. An analogous decay of the intensity at  $\lambda = 464$  nm is reported for both experiments in Fig. 5B and Fig. 6B, as well. Then, the data suggest that the model dye undergoes an analogous process of degradation during photocatalysis in the two tested media.

Therefore, we can conclude that the results suggest analogous photocatalysis mechanisms for the methyl orange dye, and that the process takes place in the herein reported Ch/PEG hydrogel as expected for a typical aqueous environment [59,77]. Also, we can infer that the electron and hole transportation occurs as widely described in literature for the N-TiO<sub>2</sub> photocatalyst synthesized by sol-gel method under visible light irradiation [50,59].

Finally, the possibility to carry out photocatalysis experiments in a

static system with no need of stirring was assessed as a key point for the following experiments with proteins as target molecules.

### 3.3. Photocatalysis of Myoglobin

Photocatalysis on biomolecules was firstly studied on the well-known model protein, Myoglobin, that was chosen as suitable biomolecular target. Myoglobin is a ubiquitous protein and its structure is conserved in proteins found in many organisms ranging from human to bacteria [85]. It is a small monomeric protein ( $\approx 18$  kDa) consisting of 153 amino acids that has been named the hydrogen atom of biology [86], and it plays an essential role in oxygen transport and storage. Its structural and functional details are well characterized. It contains a heme group with a central iron atom as prosthetic group [87], which plays an important physiological role as it binds small molecules as molecular oxygen or carbon monoxide and it can function as a scavenger against free radicals [88].

In addition, Myoglobin has been chosen as model protein to study the effects of photocatalysis by means of UV-vis absorption spectroscopy. In fact, the presence of the heme prosthetic group in its structure plays a key role in determining the spectral features of Myoglobin absorption spectrum in the visible range, such as the Soret band and the Q bands [89]. These typical bands allowed for a direct investigations of the effects of photocatalysis on Myoglobin. In addition, Myoglobin is reported to play also the biological role of scavenger in vivo because of the heme redox reactivity [88]. Therefore, there is also a further interest in elucidating how the heme group reacts with radical species during the photocatalysis process.

Myoglobin was loaded in the N-TiO<sub>2</sub>-loaded hydrogel and the UV-vis absorption measurements to test the photocatalysis effects were performed as a function of time. Importantly for the present work, the spectrum of Myoglobin in the hydrogel does not present significant differences with the one acquired in solution this suggesting no modification of the protein structure and chemistry, and confirming the suitability of the gel for protein trapping and further photocatalysis experiments. In Fig. 7, the spectral changes in the UV-vis absorption spectrum of Myoglobin embedded in N-TiO<sub>2</sub>-loaded hydrogel during irradiation are shown at different time points up to 6 h. The measurements on untreated sample ( $t = 0$ , pink line), shows the typical intense and sharp Soret band centered at around 400 nm (Fig. 7A), and the Q bands between 480 and 650 nm (Fig. 7B). The Soret peak in the visible range presents convenient properties for spectroscopic studies and the involved electronic transition is deeply understood [90–92]. The spectral profile depends on the electronic state of the molecules and in particular is sensitive to the charge, spin, and ligation state of the heme iron. Thus, modifications in Soret profile reveal changes in the configuration of the heme molecular environment and/or to the oxidation state of the molecules [93]. The so called Q bands in the heme proteins

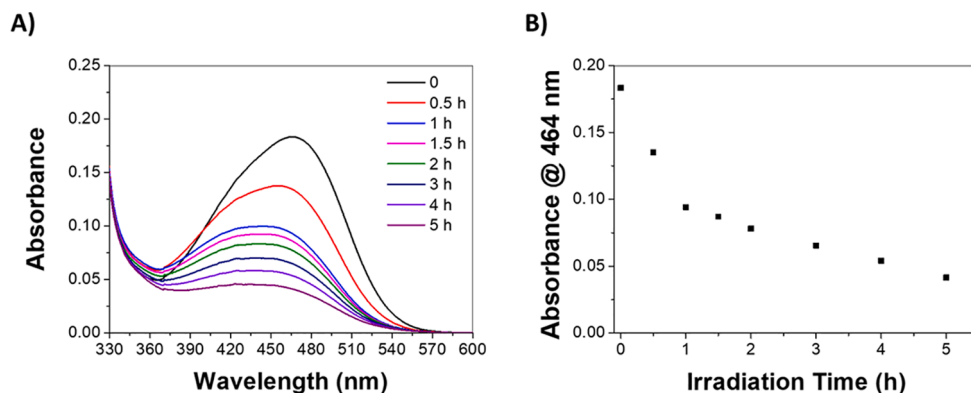


Fig. 6. A) UV-vis absorbance spectra in the range 330–600 nm for methyl orange (50 mg/L) in N-TiO<sub>2</sub>-loaded Ch/PEG hydrogel, and B) decay of the absorbance measured at  $\lambda = 464$  nm.

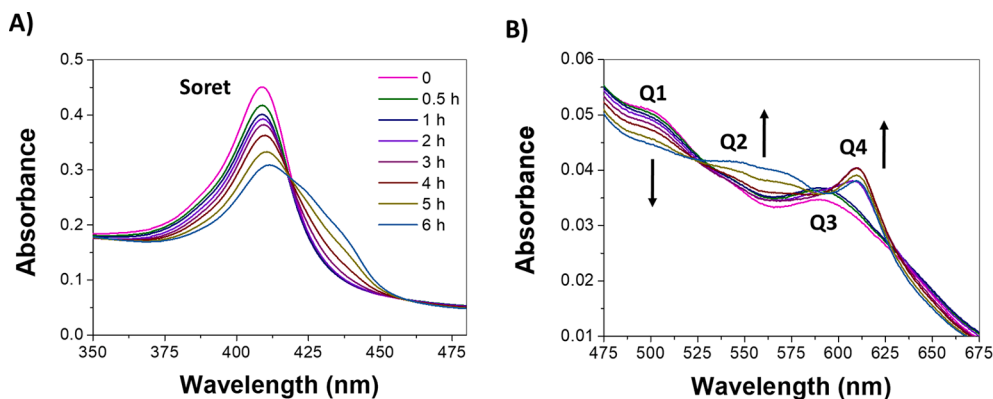


Fig. 7. UV-vis absorption spectra of Myoglobin (2 mg/mL) in 20 mg/mL N-TiO<sub>2</sub>-loaded hydrogel: A) Soret band in the spectral range of 350–475 nm, and B) Q bands in the spectral region of 475–675 nm, at different time points during irradiation under the blue light LED up to 6 h. The Q bands are labelled as Q1 to Q3 in the initial Myoglobin spectrum. A new component at  $\lambda = 610$  nm, labelled as Q4, appears during photocatalysis.

have been largely used to monitor modifications in their structure, ligand binding and redox state [89,94].

During the photocatalysis process, relevant spectral changes can be monitored both in the Soret and Q bands spectral range. Specifically, the most evident effect of photocatalysis on Myoglobin is the decrease in absorption along with a red shift on the Soret band, reported in Fig. 7A. Additionally, in the latest phase of Myoglobin photodegradation ( $t > 4$  h) the Soret band broadens, and absorption components appear in the range 420–450 nm. These changes can be ascribed both to changes in protein redox state, and to modification of the overall protein structures. It is likely that multiple reactions occur in the sample leading to critical and heterogeneous damages in Myoglobin structure.

This hypothesis is supported also by spectral changes in Q bands region, shown in Figure 7B. A complex spectral evolution upon photocatalysis was observed. At the beginning, the untreated sample presents two main peaks, at 500 nm and 590 nm, labeled as Q1 and Q3 in Figure 7B, and a less intense component Q2 at 540 nm. The Q1 peak undergoes a monotonic decrease in intensity with the irradiation time, while the Q3 peak does not seem to undergo critical modifications. After 4 h of irradiation the growth of a broad band in the range 525–590 nm is observed in the spectral range of Q2. Interestingly, a new signal, labelled as Q4 and not present in the initial Myoglobin spectrum, appears at 610 nm after 3 h of irradiation as a consequence of Myoglobin photocatalysis. These changes can be related to radical oxidation of the heme group at the iron center [95].

The interpretation of the detailed changes in protein structure is out of the scope of this work, but qualitative interpretation of the data reveal that multiple damages occur at molecular level involving at least the hydrophobic pocket surrounding the prosthetic group. Furthermore, the occurrence of the observed changes in the Q bands region, as well as for the Soret band, could be attributed to the formation of high-valent iron states, as a result of the metal oxidation due to radicals produced through the photocatalysis process, as also reported for heme synthetic derivatives in photo-oxidative reactions [87,95].

### 3.4. Photocatalysis of BSA

BSA was selected as a second model protein to assess the possibility of using the N-TiO<sub>2</sub>-loaded hydrogel matrix for the spectroscopic analysis of photocatalysis effects on biomolecules. BSA is one of the most widely studied and applied protein in biophysics, biology and biochemistry with uncountable applications in bio- and nanotechnology. It is a globular protein ( $\approx 66$  kDa) formed by a 583 amino acids single chain. The tertiary structure of this really stable protein is well defined and stabilized by 17 disulfide bonds. As the other serum albumins, it plays a key role in the transport of a large number of exogenous and endogenous ligands and it can be considered one of the main

circulating antioxidant in the blood [96,97]. BSA modifications at molecular level following photocatalysis were followed by means of steady-state fluorescence spectroscopy. The intrinsic fluorescence signal of BSA is mainly due to two tryptophans, embedded in two different domains: Trp-134, located in proximity of the protein surface, but buried in a hydrophobic pocket of domain I, and Trp-214, located in an internal part of domain II [98]. The intrinsic fluorescence can be easily monitored over time during photocatalysis with high sensitivity, and enables to obtain information on both chemical and structural changes at the tryptophan residues. Indeed, the intrinsic fluorescence of BSA can be modified as a consequence of chemical reactions at the aromatic residues, or by protein unfolding, which can be monitored through the solvatochromism of the tryptophan indole fluorophore, whose fluorescence is sensitive to changes in the local microenvironments [99,100].

Firstly, the sensitivity of fluorescence was exploited to reveal conformational changes of the protein when loaded in the hydrogel. In Fig. 8A, the fluorescence spectra of BSA in aqueous solution, in the Ch/PEG hydrogel and in the N-TiO<sub>2</sub>-loaded Ch/PEG hydrogel are reported. These measurements are aimed at highlighting possible effects of encapsulation and direct interaction with N-TiO<sub>2</sub> structures.

As shown, the protein fluorescence maximum at 342 nm observed in aqueous solution is red shifted to 346 nm upon loading in the hydrogel matrix (Fig. 8A, inset). This effect can be attributed to the slight conformational changes of the protein due to different environment [101]. The observation that the intrinsic fluorescence of peak of the protein embedded in the hydrogels is narrower than the one measured in solution is consistent with protein encapsulation in a more rigid environment. The spectral profile of the fluorescence emission band is not modified by the presence of N-TiO<sub>2</sub> particles in the gel. This suggests a minimal interaction of the protein with N-TiO<sub>2</sub> as embedded in the hydrogel, avoiding adsorption and undesired unfolding at the photocatalyst interface.

The BSA loaded in the N-TiO<sub>2</sub>-loaded Ch/PEG hydrogel was exposed to the blue light LED to activate the photocatalytic process. The time evolution of BSA fluorescence emission spectrum as a function of irradiation time is reported in Fig. 8B. As can be seen, fluorescence intensity monotonically decreases as a function of time. Decrease in fluorescence intensity was previously observed for BSA and attributed to partial unfolding of the protein following denaturation, aggregation or degradation [99,102–104]. Thus, it is possible to attribute changes in protein conformation to photocatalytic effects occurring in the N-TiO<sub>2</sub>-loaded hydrogel. These changes may be due to chemical modifications of specific target residues, which in turn modify Trp environment.

## 4. Conclusions

In the present study, the photocatalytic activity of N-TiO<sub>2</sub> particles

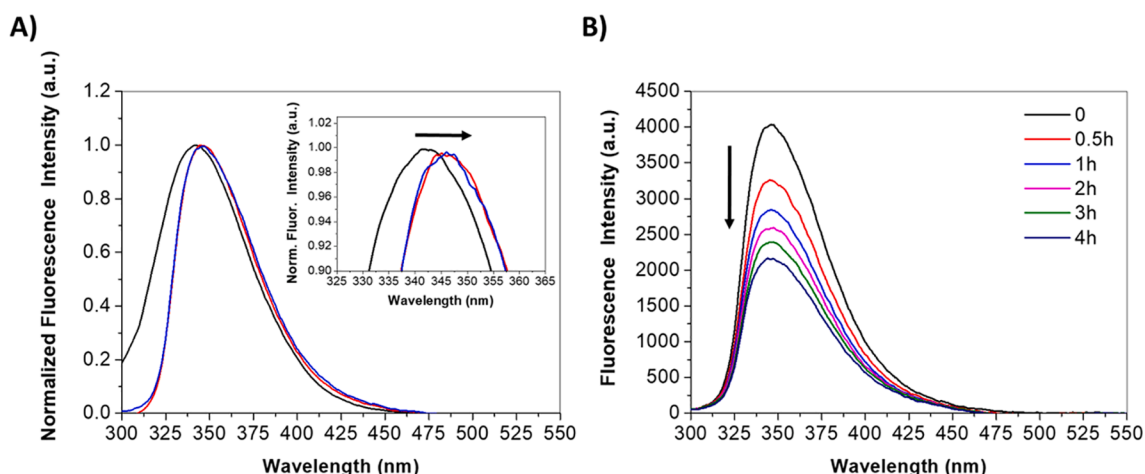


**Fig. 8.** A) Normalized fluorescence spectra of BSA (1 mg/mL) in aqueous solution (black), in Ch/PEG hydrogel (red), and in 20 mg/mL N-TiO<sub>2</sub>-loaded hydrogel (blue) recorded in the range 300–550 nm. Inset: zoom of the emission maxima; B) Decay of fluorescence intensity of BSA (1 mg/mL) in N-TiO<sub>2</sub>-loaded hydrogel at different time points during irradiation under the blue light LED up to 4 h. Data reported in (B) are obtained from fluorescence spectra normalized respect to the absorption at  $\lambda = 280$  nm. The changes in the fluorescence signal cannot be attributed to self-absorption of light in the sample as the absorption is 0.5 at the  $\lambda_{\text{ex}} = 280$  nm and less than 0.1 at  $\lambda_{\text{em}} = 345$  nm.

embedded in Ch/PEG hydrogel on globular proteins was analyzed. The N-TiO<sub>2</sub> particles were successfully produced by a sol-gel synthesis in presence of urea as a nitrogen source. The combination of the N-doping along with the nanoscale structure of the synthesized N-TiO<sub>2</sub> led to an ideal material for photocatalysis of biomolecule with good catalytic activity under blue light irradiation. The obtained N-TiO<sub>2</sub> powder was dispersed in a biocompatible chitosan hydrogel, which represents an ideal matrix for both photocatalyst and biomolecules loading. The chitosan hydrogel is characterized by good biocompatibility and transparency in the visible range, ideal features for biological investigations through a spectroscopic approach. We observed photocatalysis effects induced by visible light illumination in standard model systems like methyl orange and target proteins, such as Myoglobin and BSA. The high transparency and the stability of the gel against photocatalysis allowed a direct *in situ* investigation of protein modifications upon photocatalysis by the use of readily accessible methods, as UV-vis and fluorescence spectroscopies, with no need of protein recovery steps before the spectral analysis, avoiding undesired protein loss and structural changes. This may allow detailed analysis in real time of specific target systems which may be relevant for the advancement of photocatalysis-based strategies to face relevant biomedical issues, such as the design of antitumoral and antimicrobial platforms. This work opens up the possibility to easily study the effects of photocatalysis on biomolecules and more complex biological structures at molecular level. In particular, this photocatalytic material is found to induce, under visible irradiation, critical multitarget damages in the hydrophobic pocket surrounding the prosthetic group in Myoglobin and on the oxidation state of iron. Fluorescence measurements indicate that photocatalysis readily induces BSA unfolding. These damages clearly alter molecular structure of these biological molecules and as a consequence their function. This together with the good mechanical properties of the material, such as good resistance and spreadability, the reported N-TiO<sub>2</sub>-loaded hydrogel presents promising features towards the realization of a new photoactive hydrogel for topical antimicrobial applications in the field of phototherapy, e.g. treatments of skin infections and biofilm degradation.

#### CRedit authorship contribution statement

**Vittorio Ferrara:** Writing – original draft, Methodology, Investigation, Formal analysis, Data curation, Conceptualization. **Marco Marchetti:** Methodology, Investigation. **Domenico Alfieri:** Methodology, Investigation. **Lorenzo Targetti:** Resources, Project administration,

Funding acquisition. **Michelangelo Scopelliti:** Writing – review & editing, Methodology, Formal analysis. **Bruno Pignataro:** Writing – review & editing, Formal analysis. **Francesco Pavone:** Project administration, Funding acquisition, Conceptualization. **Valeria Vetri:** Writing – review & editing, Supervision, Project administration, Methodology, Funding acquisition, Data curation, Conceptualization. **Giuseppe Sancataldo:** Writing – review & editing, Supervision, Methodology, Investigation, Data curation, Conceptualization.

#### Declaration of Competing Interest

The authors declare the following financial interests/personal relationships which may be considered as potential competing interests:

Marco Marchetti reports a relationship with Emoled s.r.l. that includes: funding grants. Domenico Alfieri reports a relationship with Emoled S.r.l. that includes: funding grants. Lorenzo Targetti reports a relationship with Emoled s.r.l. that includes: board membership. Francesco Pavone reports a relationship with Emoled s.r.l. that includes: consulting or advisory.

The remaining authors declare that they have no known competing financial interests or personal relationships that could have appeared to influence the work reported in this paper.

#### Data availability

Data will be made available on request.

#### Acknowledgments

The authors thank Prof. Leone for useful discussions. The authors thank the University of Palermo for financial support (FFR – PROMETA project and CON-0335 - BioSAFEty Nanosystems for bacterial free SURFaces). GS has received funding from PON AIM1809078-1. Scanning Electron Microscopy, Atomic Force Microscopy and X Ray Photoelectron Spectroscopy measurements were performed at the ATen Center laboratories at the University of Palermo.

#### Appendix A. Supplementary data

Supplementary data to this article can be found online at <https://doi.org/10.1016/j.jphotochem.2022.114451>.

## References

- [1] J. You, C.-C. Chen, L. Dou, S. Murase, H.-S. Duan, S.A. Hawks, T. Xu, H.J. Son, L. Yu, G. Li, Y. Yang, Metal oxide nanoparticles as an electron-transport layer in high-performance and stable inverted polymer solar cells, *Adv. Mater.* 24 (2012) 5267–5272, <https://doi.org/10.1002/adma.201201958>.
- [2] B. O'Regan, M. Grätzel, A low-cost, high-efficiency solar cell based on dye-sensitized colloidal TiO<sub>2</sub> films, *Nature* 353 (1991) 737–740, <https://doi.org/10.1038/353737a0>.
- [3] V. Robbiano, G.M. Paternò, G.F. Cotella, T. Fiore, M. Dianetti, M. Scopelliti, F. Brunetti, B. Pignataro, F. Cacialli, Polystyrene nanoparticle-templated hollow titania nanosphere monolayers as ordered scaffolds, *J. Mater. Chem. C* 6 (2018) 2502–2508, <https://doi.org/10.1039/C7TC04070A>.
- [4] M.F. La Russa, S.A. Ruffolo, N. Rovella, C.M. Belfiore, A.M. Palermo, M.T. Guzzi, G.M. Crisci, Multifunctional TiO<sub>2</sub> coatings for cultural heritage, *Prog. Org. Coatings* 74 (2012) 186–191, <https://doi.org/10.1016/j.porgcoat.2011.12.008>.
- [5] Y. Aleeva, V. Ferrara, A. Bonasera, D.F. Chillura Martino, B. Pignataro, Superhydrophobic TiO<sub>2</sub>/fluorinated polysiloxane hybrid coatings with controlled morphology for solar photocatalysis, *Colloids Surfaces A Physicochem. Eng. Asp.* 631 (2021), 127633, <https://doi.org/10.1016/j.colsurfa.2021.127633>.
- [6] C. Chiappara, G. Arrabito, V. Ferrara, M. Scopelliti, G. Sancataldo, V. Vetri, D. F. Chillura Martino, B. Pignataro, Improved photocatalytic activity of polysiloxane TiO<sub>2</sub> composites by thermally induced nanoparticle bulk clustering and dye adsorption, *Langmuir* 37 (2021) 10354–10365, <https://doi.org/10.1021/acs.langmuir.1c01475>.
- [7] M. Dahl, Y. Liu, Y. Yin, Composite titanium dioxide nanomaterials, *Chem. Rev.* 114 (2014) 9853–9889, <https://doi.org/10.1021/cr400634p>.
- [8] R. Fatima, M.N. Afridi, V. Kumar, J. Lee, I. Ali, K.H. Kim, J.O. Kim, Photocatalytic degradation performance of various types of modified TiO<sub>2</sub> against nitrophenols in aqueous systems, *J. Clean. Prod.* 231 (2019) 899–912, <https://doi.org/10.1016/j.jclepro.2019.05.292>.
- [9] H. Chen, C.E. Nanayakkara, V.H. Grassian, Titanium dioxide photocatalysis in atmospheric chemistry, *Chem. Rev.* 112 (2012) 5919–5948, <https://doi.org/10.1021/cr3002092>.
- [10] S.M. Patil, S.P. Deshmukh, A.G. Dhodamani, K.V. More, S.D. Delekar, Different strategies for modification of titanium dioxide as heterogeneous catalyst in chemical transformations, *Curr. Org. Chem.* 21 (9) (2017) 821–833, <https://doi.org/10.2174/1385272820666161013151816>.
- [11] M. Tomás-Gamasa, J.L. Mascareñas, TiO<sub>2</sub>-Based photocatalysis at the interface with biology and biomedicine, *Chembiochem* 21 (2020) 294–309, <https://doi.org/10.1002/cbic.201900229>.
- [12] K.T. Karthikeyan, A. Nithya, K. Jothivenkatchalam, Photocatalytic and antimicrobial activities of chitosan-TiO<sub>2</sub> nanocomposite, *Int. J. Biol. Macromol.* 104 (2017) 1762–1773, <https://doi.org/10.1016/j.ijbiomac.2017.03.121>.
- [13] R. Kaur, N.S. Thakur, S. Chandna, J. Bhaumik, Sustainable lignin-based coatings doped with titanium dioxide nanocomposites exhibit synergistic microbicidal and UV-blocking performance toward personal protective equipment, *ACS Sustain. Chem. Eng.* 9 (2021) 11223–11237, <https://doi.org/10.1021/acsschemeng.1c03637>.
- [14] J. Li, S. Yuan, J. Zhu, B. Van der Bruggen, High-flux, antibacterial composite membranes via polydopamine-assisted PEI-TiO<sub>2</sub>/Ag modification for dye removal, *Chem. Eng. J.* 373 (2019) 275–284, <https://doi.org/10.1016/j.cej.2019.05.048>.
- [15] J. Shi, J. Li, Y. Wang, C.Y. Zhang, TiO<sub>2</sub>-based nanosystem for cancer therapy and antimicrobial treatment: a review, *Chem. Eng. J.* 431 (2022), 133714, <https://doi.org/10.1016/j.cej.2021.133714>.
- [16] S.P. Tallós, L. Janovák, E. Nagy, Á. Deák, A. Juhász, E. Csapó, N. Buzás, I. Dékány, Adhesion and inactivation of Gram-negative and Gram-positive bacteria on photoreactive TiO<sub>2</sub>/polymer and Ag-TiO<sub>2</sub>/polymer nanohybrid films, *Appl. Surf. Sci.* 371 (2016) 139–150, <https://doi.org/10.1016/j.apsusc.2016.02.202>.
- [17] R.J. Barnes, R. Molina, J. Xu, P.J. Dobson, I.P. Thompson, Comparison of TiO<sub>2</sub> and ZnO nanoparticles for photocatalytic degradation of methylene blue and the correlated inactivation of gram-positive and gram-negative bacteria, *J. Nanoparticle Res.* 15 (2013) 1432, <https://doi.org/10.1007/s11051-013-1432-9>.
- [18] N. Kashige, Y. Kakita, Y. Nakashima, F. Miake, K. Watanabe, Mechanism of the photocatalytic inactivation of *Lactobacillus casei* phage PL-1 by titania thin film, *Curr. Microbiol.* 42 (2001) 184–189, <https://doi.org/10.1007/s002840010201>.
- [19] N. Lagopati, K. Evangelou, P. Falaras, E.-P.-C. Tsilibary, P.V.S. Vasileiou, S. Havaki, A. Angelopoulou, E.A. Pavlatou, V.G. Gorgoulis, Nanomedicine: photo-activated nanostructured titanium dioxide, as a promising anticancer agent, *Pharmacol. Ther.* 222 (2021), 107795, <https://doi.org/10.1016/j.pharmthera.2020.107795>.
- [20] E.A. Rozhkova, I. Ulasov, B. Lai, N.M. Dimitrijevic, M.S. Lesniak, T. Rajh, A high-performance nanobio photocatalyst for targeted brain cancer therapy, *Nano Lett.* 9 (2009) 3337–3342, <https://doi.org/10.1021/nl901610f>.
- [21] Y. Zhang, L. Zhou, Y. Zhang, Investigation of UV-TiO<sub>2</sub> photocatalysis and its mechanism in *Bacillus subtilis* spore inactivation, *J. Environ. Sci. (China)* 26 (2014) 1943–1948, <https://doi.org/10.1016/j.jes.2014.07.007>.
- [22] P.C. Maness, S. Smolinski, D.M. Blake, Z. Huang, E.J. Wolfrum, W.A. Jacoby, Bactericidal activity of photocatalytic TiO<sub>2</sub> reaction: toward an understanding of its killing mechanism, *Appl. Environ. Microbiol.* 65 (1999) 4094–4098, <https://doi.org/10.1128/aem.65.9.4094-4098.1999>.
- [23] G. Carré, E. Hamon, S. Ennahar, M. Estner, M.-C. Lett, P. Horvatovich, J.-P. Gies, V. Keller, N. Keller, P. Andre, J.L. Schottel, TiO<sub>2</sub> photocatalysis damages lipids and proteins in *Escherichia coli*, *Appl. Environ. Microbiol.* 80 (8) (2014) 2573–2581.
- [24] H.A. Foster, I.B. Ditta, S. Varghese, A. Steele, Photocatalytic disinfection using titanium dioxide: spectrum and mechanism of antimicrobial activity, *Appl. Microbiol. Biotechnol.* 90 (2011) 1847–1868, <https://doi.org/10.1007/s00253-011-3213-7>.
- [25] E. Parra-Ortiz, S. Malekhaat Häffner, T. Saerbeck, M.W.A. Skoda, K. L. Browning, M. Malmsten, Oxidation of polyunsaturated lipid membranes by photocatalytic titanium dioxide nanoparticles: role of pH and salinity, *ACS Appl. Mater. Interfaces* 12 (2020) 32446–32460, <https://doi.org/10.1021/acsmi.0c08642>.
- [26] M.H. Ahmed, T.E. Keyes, J.A. Byrne, C.W. Blackledge, J.W. Hamilton, Adsorption and photocatalytic degradation of human serum albumin on TiO<sub>2</sub> and Ag-TiO<sub>2</sub> films, *J. Photochem. Photobiol. A Chem.* 222 (2011) 123–131, <https://doi.org/10.1016/j.jphotochem.2011.05.011>.
- [27] D.T. Jayaram, S. Runa, M.L. Kemp, C.K. Payne, Nanoparticle-induced oxidation of corona proteins initiates an oxidative stress response in cells, *Nanoscale* 9 (2017) 7595–7601, <https://doi.org/10.1039/c6nr09500c>.
- [28] M. Garvas, A. Testen, P. Umek, A. Gloter, T. Koklik, J. Strancar, E.A. Rozhkova, Protein corona prevents TiO<sub>2</sub> phototoxicity, *PLoS One* 10 (6) (2015) e0129577, <https://doi.org/10.1371/journal.pone.0129577>.
- [29] H. Lachheb, F. Dapozze, A. Hous, C. Guillard, Adsorption and photocatalytic degradation of cysteine in presence of TiO<sub>2</sub>, *J. Photochem. Photobiol. A Chem.* 246 (2012) 1–7, <https://doi.org/10.1016/j.jphotochem.2012.06.004>.
- [30] S. Makumire, V.S.K. Chakravadhanula, G. Köllisch, E. Redel, A. Shonhai, Immunomodulatory activity of zinc peroxide (ZnO<sub>2</sub>) and titanium dioxide (TiO<sub>2</sub>) nanoparticles and their effects on DNA and protein integrity, *Toxicol. Lett.* 227 (2014) 56–64, <https://doi.org/10.1016/j.toxlet.2014.02.027>.
- [31] C.W. Dunnill, I.P. Parkin, Nitrogen-doped TiO<sub>2</sub> thin films: photocatalytic applications for healthcare environments, *Dalt Trans* 40 (2011) 1635–1640, <https://doi.org/10.1039/c0dt00494d>.
- [32] S. Hirakura, T. Kobayashi, S. Ono, Y. Oaki, H. Imai, Fibrous nanocrystals of hydroxyapatite loaded with TiO<sub>2</sub> nanoparticles for the capture and photocatalytic decomposition of specific proteins, *Colloids Surf. B Biointerfaces* 79 (2010) 131–135, <https://doi.org/10.1016/j.colsurfb.2010.03.041>.
- [33] I. Liu, L.A. Lawton, D.W. Bahnemann, P.K.J. Robertson, The photocatalytic destruction of the cyanotoxin, nodularin using TiO<sub>2</sub>, *Appl. Catal. B Environ.* 60 (2005) 245–252, <https://doi.org/10.1016/j.apcatb.2005.03.006>.
- [34] K.A. Gebru, C. Das, Removal of bovine serum albumin from wastewater using fouling resistant ultrafiltration membranes based on the blends of cellulose acetate, and PVP-TiO<sub>2</sub> nanoparticles, *J. Environ. Manage.* 200 (2017) 283–294, <https://doi.org/10.1016/j.jenvman.2017.05.086>.
- [35] S. Loreto, B. Cuyppers, J. Brokken, S. Van Doorslaer, K. De Wael, V. Meynen, The effect of the buffer solution on the adsorption and stability of horse heart myoglobin on commercial mesoporous titanium dioxide: a matter of the right choice, *PCCP* 19 (2017) 13503–13514, <https://doi.org/10.1039/c6cp08585g>.
- [36] S. Bratskaya, Y. Privar, D. Nesterov, E. Modin, M. Kodess, A. Slobodyuk, D. Marinin, A. Pestov, Chitosan gels and cryogels cross-linked with diglycidyl ethers of ethylene glycol and polyethylene glycol in acidic media, *Biomacromolecules* 20 (4) (2019) 1635–1643.
- [37] A.E. Mohamed, W.E. Elgammal, A.M. Eid, A.M. Dawaba, A.G. Ibrahim, A. Fouda, S.M. Hassan, Synthesis and characterization of new functionalized chitosan and its antimicrobial and in-vitro release behavior from topical gel, *Int. J. Biol. Macromol.* 207 (2022) 242–253, <https://doi.org/10.1016/j.ijbiomac.2022.02.173>.
- [38] M. Mesgari, A.H. Aalami, A. Sahebkar, Antimicrobial activities of chitosan/titanium dioxide composites as a biological nanolayer for food preservation: a review, *Int. J. Biol. Macromol.* 176 (2021) 530–539, <https://doi.org/10.1016/j.ijbiomac.2021.02.099>.
- [39] T. Kamal, Y. Anwar, S.B. Khan, M.T.S. Chani, A.M. Asiri, Dye adsorption and bactericidal properties of TiO<sub>2</sub>/chitosan coating layer, *Carbohydr. Polym.* 148 (2016) 153–160, <https://doi.org/10.1016/j.carbpol.2016.04.042>.
- [40] F. Librizzi, V. Foderà, V. Vetri, C. Lo Presti, M. Leone, Effects of confinement on insulin amyloid fibrils formation, *Eur. Biophys. J.* 36 (2007) 711–715, <https://doi.org/10.1007/s00249-007-0137-3>.
- [41] C. LoPresti, V. Vetri, M. Ricca, V. Foderà, G. Tripodo, G. Spadaro, C. Dispenza, Pulsatile protein release and protection using radiation-crosslinked polypeptide hydrogel delivery devices, *React. Funct. Polym.* 71 (2011) 155–167, <https://doi.org/10.1016/j.reactfunctpolym.2010.11.030>.
- [42] J.-T. Zhang, S. Petersen, M. Thunga, E. Leipold, R. Weidisch, X. Liu, A. Fahr, K. D. Jandt, Micro-structured smart hydrogels with enhanced protein loading and release efficiency, *Acta Biomater.* 6 (2010) 1297–1306, <https://doi.org/10.1016/j.actbio.2009.11.005>.
- [43] S.H. Gehrke, L.H. Uhdén, J.F. McBride, Enhanced loading and activity retention of bioactive proteins in hydrogel delivery systems, *J. Control. Release* 55 (1998) 21–33, [https://doi.org/10.1016/S0168-3659\(98\)00019-4](https://doi.org/10.1016/S0168-3659(98)00019-4).
- [44] S. Peers, A. Montebault, C. Ladavière, Chitosan hydrogels incorporating colloids for sustained drug delivery, *Carbohydr. Polym.* 275 (2022) 118689.
- [45] M. George, T.E. Abraham, Polyionic hydrocolloids for the intestinal delivery of protein drugs: alginate and chitosan — a review, *J. Control. Release* 114 (2006) 1–14, <https://doi.org/10.1016/j.jconrel.2006.04.017>.
- [46] O. Masalova, V. Kulikouskaya, T. Shutava, V. Agabekov, Alginate and chitosan gel nanoparticles for efficient protein entrapment, *Phys. Procedia* 40 (2013) 69–75, <https://doi.org/10.1016/j.phpro.2012.12.010>.

- [47] Y. Xu, Y. Du, Effect of molecular structure of chitosan on protein delivery properties of chitosan nanoparticles, *Int. J. Pharm.* 250 (2003) 215–226, [https://doi.org/10.1016/S0378-5173\(02\)00548-3](https://doi.org/10.1016/S0378-5173(02)00548-3).
- [48] C.B. Elias, J.B. Joshi, Role of Hydrodynamic Shear on Activity and Structure of Proteins BT - Bioprocess and Algae Reactor Technology, Apoptosis. Springer Berlin Heidelberg, Berlin, Heidelberg, 1998, pp. 47–71.
- [49] C.R. Thomas, D. Geer, Effects of shear on proteins in solution, *Biotechnol. Lett.* 33 (2011) 443–456, <https://doi.org/10.1007/s10529-010-0469-4>.
- [50] R. Asahi, T. Morikawa, H. Irie, T. Ohwaki, Nitrogen-doped titanium dioxide as visible-light-sensitive photocatalyst: designs, developments, and prospects, *Chem. Rev.* 114 (2014) 9824–9852, <https://doi.org/10.1021/cr5000738>.
- [51] R. López, R. Gómez, Band-gap energy estimation from diffuse reflectance measurements on sol-gel and commercial TiO<sub>2</sub>: a comparative study, *J. Sol-Gel Sci. Technol.* 61 (2012) 1–7, <https://doi.org/10.1007/s10971-011-2582-9>.
- [52] Y.A. Vladimirov, D.I. Roshchupkin, E.E. Fesenko, Photochemical reactions in amino acid residues and inactivation of enzymes during U.V.-irradiation. A review, *Photochem. Photobiol.* 11 (1970) 227–246, <https://doi.org/10.1111/j.1751-1097.1970.tb05992.x>.
- [53] H. Görner, New trends in photobiology: Photochemistry of DNA and related biomolecules: quantum yields and consequences of photoionization, *J. Photochem. Photobiol. B Biol.* 26 (1994) 117–139, [https://doi.org/10.1016/1011-1344\(94\)07068-7](https://doi.org/10.1016/1011-1344(94)07068-7).
- [54] S. Guo, S. Han, H. Mao, C. Wu, L. Jia, B. Chi, J. Pu, L. Jian, Synthesis and characterization of nitrogen and phosphate codoped titanium dioxide with excellent visible-light photocatalytic activity, *J. Alloy. Compd.* 544 (2012) 50–54, <https://doi.org/10.1016/j.jallcom.2012.07.128>.
- [55] M. Ksibi, S. Rossignol, J.M. Tatibouët, C. Trapalis, Synthesis and solid characterization of nitrogen and sulfur-doped TiO<sub>2</sub> photocatalysts active under near visible light, *Mater. Lett.* 62 (2008) 4204–4206, <https://doi.org/10.1016/j.matlet.2008.06.026>.
- [56] J. Marques, T.D. Gomes, M.A. Forte, R.F. Silva, C.J. Tavares, A new route for the synthesis of highly-active N-doped TiO<sub>2</sub> nanoparticles for visible light photocatalysis using urea as nitrogen precursor, *Catal. Today* 326 (2019) 36–45, <https://doi.org/10.1016/j.cattod.2018.09.002>.
- [57] D. Chen, Z. Jiang, J. Geng, Q. Wang, D. Yang, Carbon and nitrogen co-doped TiO<sub>2</sub> with enhanced visible-light photocatalytic activity, *Ind. Eng. Chem. Res.* 46 (2007) 2741–2746, <https://doi.org/10.1021/ie061491k>.
- [58] S. Cataldo, B.M. Weckhuysen, A. Pettignano, B. Pignataro, Multi-doped brookite-prevalent TiO<sub>2</sub> photocatalyst with enhanced activity in the visible light, *Catal. Lett.* 148 (2018) 2459–2471, <https://doi.org/10.1007/s10562-018-2463-8>.
- [59] S.A. Ansari, M.M. Khan, M.O. Ansari, M.H. Cho, Nitrogen-doped titanium dioxide (N-doped TiO<sub>2</sub>) for visible light photocatalysis, *New J. Chem.* 40 (2016) 3000–3009, <https://doi.org/10.1039/c5nj03478g>.
- [60] K.A. Schenkman, D.R. Marble, D.H. Burns, E.O. Feigl, Myoglobin oxygen dissociation by multiwavelength spectroscopy, *J. Appl. Physiol.* 82 (1997) 86–92, <https://doi.org/10.1152/jappp.1997.82.1.86>.
- [61] S. Désilet, P. Brousseau, D. Chamberland, S. Singh, H. Feng, R. Turcotte, K. Armstrong, J. Anderson, Analyses of the thermal decomposition of urea nitrate at high temperature, *Thermochim. Acta* 521 (2011) 59–65, <https://doi.org/10.1016/j.tca.2011.04.004>.
- [62] Z. Cheng, Z. Gu, J. Chen, J. Yu, L. Zhou, Synthesis, characterization, and photocatalytic activity of porous La–N-co-doped TiO<sub>2</sub> nanotubes for gaseous chlorobenzene oxidation, *J. Environ. Sci.* 46 (2016) 203–213, <https://doi.org/10.1016/j.jes.2015.09.026>.
- [63] P. Praveen, G. Viruthagiri, S. Mugundan, N. Shanmugam, Structural, optical and morphological analyses of pristine titanium di-oxide nanoparticles - Synthesized via sol-gel route, *Spectrochim. Acta - Part A Mol. Biomol. Spectrosc.* 117 (2014) 622–629, <https://doi.org/10.1016/j.saa.2013.09.037>.
- [64] P. Tao, Y. Li, A. Rungta, A. Viswanath, J. Gao, B.C. Benicewicz, R.W. Siegel, L. S. Schadler, TiO<sub>2</sub> nanocomposites with high refractive index and transparency, *J. Mater. Chem.* 21 (2011) 18623–18629, <https://doi.org/10.1039/c1jm13093e>.
- [65] G. Yang, Z. Jiang, H. Shi, T. Xiao, Z. Yan, Preparation of highly visible-light active N-doped TiO<sub>2</sub> photocatalyst, *J. Mater. Chem.* 20 (2010) 5301–5309, <https://doi.org/10.1039/c0jm00376j>.
- [66] J. Du, G. Zhao, Y. Shi, HaoYang, Y. Li, G. Zhu, Y. Mao, R. Sa, W. Wang, A facile method for synthesis of N-doped TiO<sub>2</sub> nanooctahedra, nanoparticles, and nanospheres and enhanced photocatalytic activity, *Appl. Surf. Sci.* 273 (2013) 278–286.
- [67] X. Wang, K. Zhang, X. Guo, G. Shen, J. Xiang, Synthesis and characterization of N-doped TiO<sub>2</sub> loaded onto activated carbon fiber with enhanced visible-light photocatalytic activity, *New J. Chem.* 38 (2014) 6139–6146, <https://doi.org/10.1039/c4nj00962b>.
- [68] C. Guiot, O. Spalla, Stabilization of TiO<sub>2</sub> nanoparticles in complex medium through a pH adjustment protocol, *Environ. Sci. Tech.* 47 (2013) 1057–1064, <https://doi.org/10.1021/es3040736>.
- [69] N.Y. Joo, J. Lee, S.J. Kim, S.H. Hong, H.M. Park, W.S. Yun, M. Yoon, N.W. Song, Preparation of an aqueous suspension of stabilized TiO<sub>2</sub> nanoparticles in primary particle form, *J. Nanosci. Nanotechnol.* 13 (2013) 6153–6159, <https://doi.org/10.1166/jnn.2013.7637>.
- [70] T.A. Egerton, I.R. Tooley, Physical characterization of titanium dioxide nanoparticles, *Int. J. Cosmet. Sci.* 36 (2014) 195–206, <https://doi.org/10.1111/ics.12113>.
- [71] S.A. Simakov, Y. Tsur, Surface stabilization of nano-sized titanium dioxide: improving the colloidal stability and the sintering morphology, *J. Nanoparticle Res.* 9 (2007) 403–417, <https://doi.org/10.1007/s11051-006-9099-0>.
- [72] M. Rahimzadeh-Soltani, K. Saberyan, F. Shahri, A. Simchi, Formation mechanism of TiO<sub>2</sub> nanoparticles in H<sub>2</sub>O-assisted atmospheric pressure CVS process, *Powder Technol.* 209 (2011) 15–24, <https://doi.org/10.1016/j.powtec.2011.01.021>.
- [73] M.F. Yan, W.W. Rhodes, Low temperature sintering of TiO<sub>2</sub>, *Mater. Sci. Eng.* 61 (1983) 59–66, [https://doi.org/10.1016/0025-5416\(83\)90126-X](https://doi.org/10.1016/0025-5416(83)90126-X).
- [74] K. Dai, H. Chen, T. Peng, D. Ke, H. Yi, Photocatalytic degradation of methyl orange in aqueous suspension of mesoporous titania nanoparticles, *Chemosphere* 69 (2007) 1361–1367, <https://doi.org/10.1016/j.chemosphere.2007.05.021>.
- [75] S. Al-Qaradawi, S.R. Salman, Photocatalytic degradation of methyl orange as a model compound, *J. Photochem. Photobiol. A Chem.* 148 (2002) 161–168, [https://doi.org/10.1016/S1010-6030\(02\)00086-2](https://doi.org/10.1016/S1010-6030(02)00086-2).
- [76] K.M. Parida, N. Sahu, N.R. Biswal, B. Naik, A.C. Pradhan, Preparation, characterization, and photocatalytic activity of sulfate-modified titania for degradation of methyl orange under visible light, *J. Colloid Interface Sci.* 318 (2008) 231–237, <https://doi.org/10.1016/j.jcis.2007.10.028>.
- [77] F. Chen, H. Liu, S. Bagwasi, X. Shen, J. Zhang, Photocatalytic study of BiOCl for degradation of organic pollutants under UV irradiation, *J. Photochem. Photobiol. A Chem.* 215 (2010) 76–80, <https://doi.org/10.1016/j.jphotochem.2010.07.026>.
- [78] M.S. Nasrollahzadeh, M. Hadavifar, S.S. Ghasemi, M. Arab Chamjangali, Synthesis of ZnO nanostructure using activated carbon for photocatalytic degradation of methyl orange from aqueous solutions, *Appl. Water Sci.* 8 (2018) 104, <https://doi.org/10.1007/s13201-018-0750-6>.
- [79] R. Cai, B. Zhang, J. Shi, M. Li, Z. He, Rapid photocatalytic decolorization of methyl orange under visible light using VS4/carbon powder nanocomposites, *ACS Sustain. Chem. Eng.* 5 (2017) 7690–7699, <https://doi.org/10.1021/acssuschemeng.7b01137>.
- [80] T. Chen, Y. Zheng, J.-M. Lin, G. Chen, Study on the photocatalytic degradation of methyl orange in water using Ag/ZnO as catalyst by liquid chromatography electrospray ionization ion-trap mass spectrometry, *J. Am. Soc. Mass Spectrom.* 19 (2008) 997–1003, <https://doi.org/10.1016/j.jasms.2008.03.008>.
- [81] H. Lee, Y.-K. Park, S.-J. Kim, B.-H. Kim, H.-S. Yoon, S.-C. Jung, Rapid degradation of methyl orange using hybrid advanced oxidation process and its synergistic effect, *J. Ind. Eng. Chem.* 35 (2016) 205–210, <https://doi.org/10.1016/j.jiec.2015.12.037>.
- [82] M.U.D. Sheikh, G.A. Naikoo, M. Thomas, M. Bano, F. Khan, Solar-assisted photocatalytic reduction of methyl orange azo dye over porous TiO<sub>2</sub> nanocomposites, *New J. Chem.* 40 (2016) 5483–5494, <https://doi.org/10.1039/C5NJ03513A>.
- [83] V. Ferrara, G. Zito, G. Arrabito, S. Cataldo, M. Scopelliti, C. Giordano, V. Vetri, B. Pignataro, Aqueous processed biopolymer interfaces for single-cell microarrays, *ACS Biomater. Sci. Eng.* 6 (2020) 3174–3186, <https://doi.org/10.1021/acsbmaterials.9b01871>.
- [84] P. Falaras, I.M. Arabatzis, T. Stergiopoulos, M.C. Bernard, Enhanced activity of silver modified thin-film TiO<sub>2</sub> photocatalysts, *Int. J. Photoenergy* 5 (2003) 123–130, <https://doi.org/10.1155/S1110662X03000230>.
- [85] S. Hou, R.W. Larsen, D. Boudko, C.W. Riley, E. Karatan, M. Zimmer, G.W. Ordal, M. Alam, Myoglobin-like aerotaxis transducers in Archaea and Bacteria, *Nature* 403 (2000) 540–544, <https://doi.org/10.1038/35000570>.
- [86] H. Frauenfelder, B.H. McMahon, P.W. Fenimore, Myoglobin: the hydrogen atom of biology and a paradigm of complexity, *Proc. Natl. Acad. Sci.* 100 (15) (2003) 8615–8617.
- [87] B.K. Patel, N. Sepay, A. Mahapatra, Structural alteration of myoglobin with two homologous cationic surfactants and effect of β-cyclodextrin: multifaceted insight and molecular docking study, *New J. Chem.* 44 (2020) 19555–19569, <https://doi.org/10.1039/d0nj01113d>.
- [88] H.P. Hersleth, K.K. Andersson, How different oxidation states of crystalline myoglobin are influenced by X-rays, *Biochim. Biophys. Acta - Proteins Proteomics* 1814 (2011) 785–796, <https://doi.org/10.1016/j.bbapap.2010.07.019>.
- [89] G.J. Smith, K.P. Ghiggino, L.E. Bennett, T.L. Nero, The ‘q-band’ absorption spectra, *Photochem. Photobiol.* 49 (1989) 49–52, <https://doi.org/10.1111/j.1751-1097.1989.tb04076.x>.
- [90] B. Melchers, E.W. Knapp, F. Parak, L. Cordone, A. Cupane, M. Leone, Structural fluctuations of myoglobin from normal-modes, Mössbauer, Raman, and absorption spectroscopy, *Biophys. J.* 70 (1996) 2092–2099, [https://doi.org/10.1016/S0006-3495\(96\)79775-8](https://doi.org/10.1016/S0006-3495(96)79775-8).
- [91] A. Cupane, M. Cammarata, L. Cordone, M. Leone, E. Vitranò, N. Engler, F. Parak, Spectral broadening of the Soret band in myoglobin: an interpretation by the full spectrum of low-frequency modes from a normal modes analysis, *Eur. Biophys. J.* 34 (2005) 881–889, <https://doi.org/10.1007/s00249-004-0458-4>.
- [92] M. Leone, A. Cupane, V. Militello, L. Cordone, Thermal broadening of the Soret band in heme complexes and in heme-proteins: role of iron dynamics, *Eur. Biophys. J.* 23 (1994) 349–352, <https://doi.org/10.1007/BF00188658>.
- [93] E.S. Peterson, E.F. Leonard, J.A. Foulke, M.C. Oliff, R.D. Salisbury, D.Y. Kim, Folding myoglobin within a sol-gel glass: protein folding constrained to a small volume, *Biophys. J.* 95 (2008) 322–332, <https://doi.org/10.1529/biophysj.106.097428>.
- [94] H.Y. Cao, Y.Q. Ma, L.X. Gao, Q. Tang, X.F. Zheng, Photo induced reaction of myoglobins with energy transferred from excited free tryptophan, *RSC Adv.* 10 (2020) 43853–43858, <https://doi.org/10.1039/d0ra09341f>.
- [95] K.W. Kwong, D. Patel, J. Malone, N.F. Lee, B. Kash, R. Zhang, An investigation of ligand effects on the visible light-induced formation of porphyrin-iron(IV)-oxo intermediates, *New J. Chem.* 41 (2017) 14334–14341, <https://doi.org/10.1039/c7nj03296j>.

- [96] M. Roche, P. Rondeau, N.R. Singh, E. Tarnus, E. Bourdon, The antioxidant properties of serum albumin, *FEBS Lett.* 582 (2008) 1783–1787, <https://doi.org/10.1016/j.febslet.2008.04.057>.
- [97] G.J. Quinlan, G.S. Martin, T.W. Evans, Albumin: biochemical properties and therapeutic potential, *Hepatology* 41 (2005) 1211–1219, <https://doi.org/10.1002/hep.20720>.
- [98] V. Militello, V. Vetri, M. Leone, Conformational changes involved in thermal aggregation processes of bovine serum albumin, *Biophys. Chem.* 105 (2003) 133–141, [https://doi.org/10.1016/S0301-4622\(03\)00153-4](https://doi.org/10.1016/S0301-4622(03)00153-4).
- [99] D.M. Togashi, A.G. Ryder, D. O'Shaughnessy, Monitoring local unfolding of bovine serum albumin during denaturation using steady-state and time-resolved fluorescence spectroscopy, *J. Fluoresc.* 20 (2010) 441–452, <https://doi.org/10.1007/s10895-009-0566-8>.
- [100] G.S. Loving, M. Sainlos, B. Imperiali, Monitoring protein interactions and dynamics with solvatochromic fluorophores, *Trends Biotechnol.* 28 (2010) 73–83, <https://doi.org/10.1016/j.tibtech.2009.11.002>.
- [101] J.R. Lakowicz (Ed.), *Principles of Fluorescence Spectroscopy*, Springer US, Boston, MA, 2006.
- [102] V. Vetri, F. Librizzi, M. Leone, V. Militello, Thermal aggregation of bovine serum albumin at different pH: comparison with human serum albumin, *Eur. Biophys. J.* 36 (2007) 717–725, <https://doi.org/10.1007/s00249-007-0196-5>.
- [103] V. Vetri, M. D'Amico, V. Foderà, M. Leone, A. Ponzoni, G. Sberveglieri, V. Militello, Bovine Serum Albumin protofibril-like aggregates formation: Solo but not simple mechanism, *Arch. Biochem. Biophys.* 508 (2011) 13–24, <https://doi.org/10.1016/j.abb.2011.01.024>.
- [104] G. Sancataldo, V. Vetri, V. Foderà, G. Di Cara, V. Militello, M. Leone, Oxidation enhances human serum albumin thermal stability and changes the routes of amyloid fibril formation, *PLoS One* 9 (2014) e84552.